Materials Horizons

A Tetrathienopyrrole-Based Ladder-Type Donor Polymer for High-Performance Organic Near-Infrared Cavity Detectors

Journal:	*Materials Horizons*
Manuscript ID	MH-COM-07-2023-001010.R1
Article Type:	Communication
Date Submitted by the Author:	19-Sep-2023
Complete List of Authors:	Valkeneers, Kaat; Hasselt University, Department of Chemistry Raymakers, Jorne; UHasselt, Chemistry Liu, Quan; UHasselt, Physics Vanderspikken, Jochen; Hasselt University Faculty of Sciences, Wang, Yuming; Hasselt University, Physics Kesters, Jurgen; Hasselt University, Institute for Materials Research (IMO-IMOMEC), Design & Synthesis of Organic Semiconductors (DSOS) Quill, Tyler; Stanford University Liu, Zhen; Vrije Universiteit Brussel Van den Brande, Niko; Vrije Universiteit Brussel, Materials and Chemistry Lutsen, Laurence; Hasselt University Vandewal, Koen; Universiteit Hasselt Faculteit Wetenschappen, IMO/IMOMEC Maes, Wouter; UHasselt, Chemistry

Incorporation of NIR detectors into wearable and handheld devices opens up many exciting applications, such as on-the-spot medical diagnostics. To extend beyond the detection window of silicon, i.e. 1000 nm, organic semiconductors are highly attractive because of their tunable absorption. However, for each targeted NIR range, this requires individually optimized materials. Moreover, finding molecules with strong absorption >1 μm that perform well in photodetectors is not trivial. This challenge can be addressed by a clever device design. Pioneering work by some of us (K. Vandewal, *Nat. Commun.* **2017**, *8*, 15421) has shown that a resonant optical microcavity allows to greatly enhance the EQE of the intermolecular charge-transfer absorption at the resonance wavelength, allowing for narrowband NIR photodetection. To date, this approach has provided the highest peak specific detectivities >1200 nm using organic semiconductors. Nevertheless, the performance can be raised significantly by the design of novel donor and acceptor materials, as shown here. By extending the π-conjugated backbone of a particular donor polymer, higher hole mobility and better intermixing in the active layer are achieved, leading to enhanced peak EQEs up to 1450 nm and record-high detectivities (1.07×10^{12} to 1.82×10^{10} Jones) in the 900–1400 nm wavelength regime.

A Tetrathienopyrrole-Based Ladder-Type Donor Polymer for High-Performance Organic Near-Infrared Cavity Detectors

Kaat Valkeneers[a,b,c,†], Jorne Raymakers[a,b,c,†], Quan Liu[a,b,c,*], Jochen Vanderspikken[a,b,c], Yuming Wang[a,b,c], Jurgen Kesters[a,b,c], Tyler James Quill[d], Zhen Liu[e], Niko Van den Brande[e], Laurence Lutsen[a,b,c], Koen Vandewal[a,b,c,*], Wouter Maes[a,b,c,*]

[a] *Hasselt University, Institute for Materials Research (IMO), Agoralaan Building D, 3590 Diepenbeek, Belgium*
[b] *IMEC, Associated Lab IMOMEC, Wetenschapspark 1, 3590 Diepenbeek, Belgium*
[c] *Energyville, Thorpark, 3600 Genk, Belgium*
[d] *Stanford University, Department of Materials Science and Engineering, Stanford, CA 94305, USA*
[e] *Vrije Universiteit Brussel, Physical Chemistry and Polymer Science, Pleinlaan 2, 1050 Brussels, Belgium*
† *These authors contributed equally.*

Abstract

Organic semiconductors can afford detection at wavelengths beyond commercial silicon photodetectors. However, for each targeted near-infrared wavelength range, this requires individually optimized materials, which adds to the complexity and costs. Moreover, finding molecules with strong absorption beyond 1 μm that perform well in organic photodetectors remains a challenge. In microcavity devices, the detection window can be extended to wavelengths inaccessible for silicon without the need for new materials by adopting an intelligent design. Previous work has demonstrated the applicability of a dithienopyrrole-based donor polymer (PDTPQx) in such a cavity photodetector device, with a photoresponse up to 1200 nm. In this work, the π-conjugated backbone of the polymer is extended, affording higher hole mobility and better donor:acceptor intermixing. This leads to enhanced peak external quantum efficiencies up to 1450 nm. The (thermal noise limited) detectivities achieved with the PTTPQx polymer (1.07×10^{12} to 1.82×10^{10} Jones) are among the very best in the 900–1400 nm wavelength regime.

Introduction

Even though near-infrared (NIR) light is invisible to the human eye, NIR photodetectors are used in numerous applications, such as medical monitoring,[1,2] industrial inspection,[3,4] biomedical sensing,[5,6] and environmental surveillance.[7,8] Commercialized NIR photodetectors rely primarily on single-crystal inorganic materials such as silicon[9] or InGaAs[10] but suffer from complex and costly processing requirements. Furthermore, the performance of silicon-based detectors is limited to wavelengths of ~900 nm because of silicon's wide bandgap.[11] Organic materials do not have these drawbacks and their absorption can be extended further into the NIR by tuning the bandgap *via* synthetic modifications.[12] Many different NIR-absorbing organic small molecule and polymer compounds have been prepared and some of these have been proven to be useful for NIR organic photodetectors (OPDs) in a wavelength range inaccessible for silicon.[13–19] However, for each targeted wavelength (range), new molecules have to be developed, which is a very time consuming and costly process.

An alternative approach to extend and enhance the detectivity in the NIR without the need for new materials employs innovative device architectures.[15] One particular method uses the filtering effect in thick polymer layers, known as charge collection narrowing (CCN).[20–22] However, this still requires the synthesis of innovative narrow-gap compounds to reach far in the NIR. Other strategies try to enhance the low-gap but low-intensity intermolecular charge-transfer (CT) absorption between two organic materials. In a typical broadband OPD device based on an organic donor-acceptor bulk heterojunction, photon absorption is the result of an electronic transition from the highest occupied molecular orbital (HOMO) to the lowest unoccupied molecular orbital (LUMO) in either the donor or acceptor material. CT absorption, on the other hand, results from an intermolecular transition between the HOMO of the donor and the LUMO of the acceptor. This type of absorption, which occurs at the donor-acceptor interface, is usually two orders of magnitude less intense than singlet absorption. In 2018, however, a new device architecture was proposed, where two (partly) reflecting electrodes are used in combination with an optically thick active layer.[23] In this way, a resonant optical microcavity is created which can greatly enhance the external quantum efficiency (EQE) of the CT absorption at the resonance wavelength, allowing for narrowband photodetection. To date, this approach has provided the highest peak specific detectivities in the wavelength range beyond 1200 nm using organic semiconductors.[15–17]

Earlier work showed that the full-width-at-half-maximum (FWHM) of the optical response peak of the microcavity device is proportional to the CT absorption strength.[24] A narrowband response therefore benefits from the weak nature of the CT transition. However, when CT absorption is too weak, parasitic absorption within the reflecting electrodes will diminish the peak EQE value. Thus, there is an optimal CT absorption strength, which was previously achieved using PBTTT-type polymers[25,26] blended with the methanofullerene $PC_{61}BM$.

Last year, our group reported the synthesis of a 'high-HOMO' dithieno[3,2-*b*:2',3'-*d*]pyrrole (DTP) based copolymer (PDTPQx, **Figure 1**) and its application in such a microcavity device,[27] achieving photodetection for wavelengths up to 1200 nm. In the present work, two additional thiophene units were fused to the electron-rich building block, resulting in an extended 'tetrathienopyrrole' (TTP) monomer and the analogous polymer PTTPQx (**Figure 1**). Elongated 'ladder-type' π-conjugated systems are expected to reduce the reorganization energy, since a more rigid conjugated structure is less prone to molecular geometry modifications upon charge carrier injection, which enhances the charge-transport ability.[28,29] Furthermore, it facilitates orderly solid-state organization and affords strong intermolecular interactions.[30,31] When combined with $PC_{61}BM$, the PTTPQx polymer showed sufficiently strong CT absorption at wavelengths beyond 1300 nm and outperformed PDTPQx in

photodiodes. Applied into a microcavity OPD device, PTTPQx:$PC_{61}BM$ blends showed among the highest specific detectivities of 1.07 x 10^{12} to 1.82 x 10^{10} Jones in the wavelength range between 900 and 1400 nm as compared to the current state-of-the art OPDs, a 15-fold improvement with respect to the analogous DTP-based donor polymer.

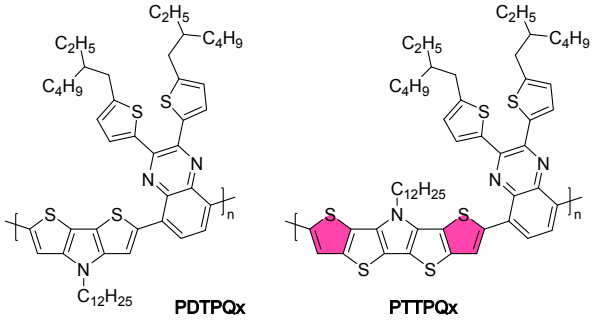

Figure 1: Chemical structures of the donor polymers PDTPQx (left) and PTTPQx (right).

Results and discussion

The electron-rich TTP monomer was synthesized following a (adapted) procedure reported by Bauerle *et al.* (**Scheme 1**).[32] 3-Bromothieno[3,2-*b*]thiophene (**4**), synthesized according to literature,[33] was homocoupled using lithium diisopropylamide and copper(II) chloride. Thereafter, a double Buchwald-Hartwig amination was carried out to obtain the TTP structure. We observed that after 24 hours of reflux in toluene, a lot of unreacted starting material remained. Therefore, an additional amount of the catalyst was added and the reaction was heated to reflux once again and continued overnight. Furthermore, it was noticed that the purity of precursor **5** was crucial to obtain a reasonable yield for the Buchwald-Hartwig reaction. No impurities could be seen by NMR but a yellow contaminant remained present. Only after repeated recrystallization and column chromatography, this could be removed and compound **5** was obtained as a fluffy off-white solid. Using this extensively purified product, the final TTP compound was obtained in 65% yield. Stannylation was carried out according to a standard procedure using *n*-butyllithium and trimethyltin chloride. The distannylated TTP monomer **7** was then copolymerized with a bromine-flanked quinoxaline (Qx) monomer (synthesized according to literature)[34] *via* a standard Stille cross-coupling polymerization (applying Pd_2dba_3 and P(*o*-tol)$_3$ as the catalytic system). Experimental details for all synthesis efforts and NMR spectra for the TTP monomer are provided in the Electronic Supplementary Information (ESI) (**Figure S1-2**).

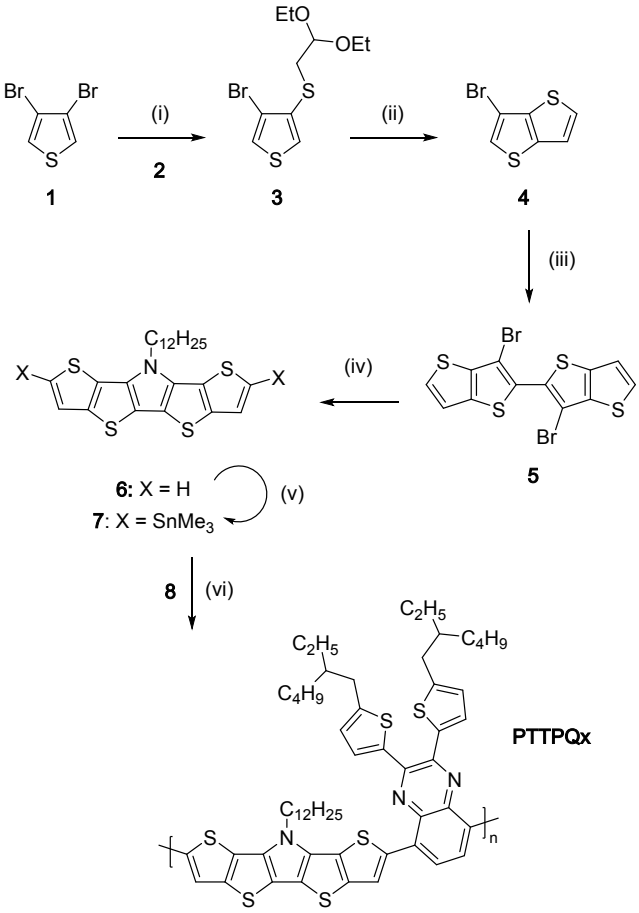

Scheme 1: Synthesis of PTTPQx. (i) *t*-BuLi, 1,2-bis(2,2-diethoxyethyl)disulphide (**2**), Et_2O (81%); (ii) Amberlyst 15, Et_2O (69%); (iii) LDA, $CuCl_2$, THF (48%); (iv) Pd_2dba_3, BINAP, *t*-BuONa, dodecylamine, toluene (65%); (v) *n*-BuLi, Me_3SnCl, THF (61%); (vi) 5,8-dibromo-2,3-bis[5-(2-ethylhexyl)thiophen-2-yl]quinoxaline (**8**), Pd_2dba_3, P(*o*-tol)$_3$, chlorobenzene (50%).

An overview of the polymer properties and a comparison to the analogous DTP copolymer is given in **Table 1**. The structure of PTTPQx was confirmed by matrix-assisted laser desorption/ionization - time of flight (MALDI-ToF) mass spectrometry (**Figure S4**) and analysis by high-temperature gel permeation chromatography (GPC) indicated a number average molar mass (M_n) of 12.8 kg mol^{-1} with a dispersity ($Đ$) of 2.3 (compared to 19.9 kg mol^{-1} for PDTPQx). Cyclic voltammetry (CV) measurements were performed to estimate the frontier molecular orbital energy levels (**Figure S5**). HOMO and LUMO levels of –4.76 and –3.22 eV were found, respectively, almost identical to the values obtained for PDTPQx (–4.79 and –3.23 eV, respectively).[27] The thermal properties of PTTPQx were studied *via* thermogravimetric analysis (TGA) and rapid heat-cool calorimetry (RHC) (**Figure S6**). Minor mass loss was observed from *ca.* 300 °C, while RHC showed no clear thermal transitions, suggesting a rather amorphous polymer nature. The UV-Vis-NIR absorption spectra gave a similar absorption for both polymers (**Figure 2**), with peak maxima in film at 773 nm. Minimal spectral changes were observed for PTTPQx when left open at the air in solution for a week (**Figure S7**).

Table 1: Overview of the molar mass, optical, and electrochemical properties of PDTPQx and PTTPQx.

Polymer	M_n[a]	Đ [a]	$\lambda_{max,film}$[b]	E_{red}[c]	E_{ox}[c]	E_{LUMO}[d]	E_{HOMO}[d]	$E_{g,CV}$[e]	$E_{g,opt}$[f]
	(kg mol^{-1})		(nm)	(V)	(V)	(eV)	(eV)	(eV)	(eV)
PDTPQx	19.9	2.6	773	–1.67	–0.10	–3.23	–4.79	1.57	1.39
PTTPQx	12.8	2.3	773	–1.68	–0.14	–3.22	–4.76	1.54	1.39

[a] Determined by GPC at 160 °C in 1,2,4-trichlorobenzene. [b] Films were prepared by drop-casting a polymer solution from chloroform onto a quartz disc. [c] Onset potentials vs. Fc/Fc^+. [d] Determined from the onset of oxidation/reduction in CV. [e] Electrochemical bandgap. [f] Optical bandgap, determined by the onset of the solid-state UV-Vis-NIR absorption spectrum.

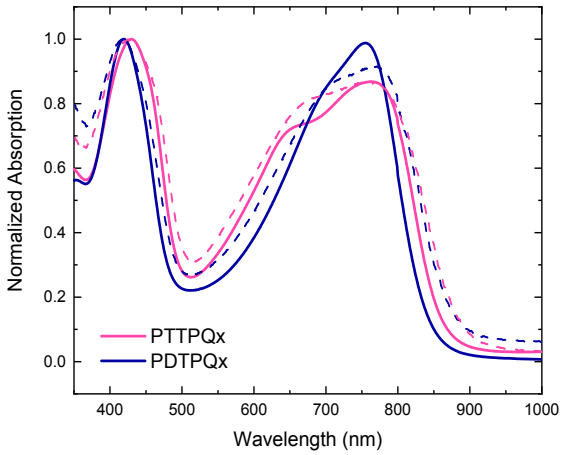

Figure 2: Normalized UV-Vis-NIR absorption spectra for PDTPQx (blue) and PTTPQx (pink) in solution (solid line) and in film (dashed line).

To determine the effect of the extended conjugated backbone on the photodiode characteristics, inverted device stacks (ITO/ZnO/PTTPQx:$PC_{61}BM$/MoO_3/Ag) containing the PTTPQx polymer in combination with $PC_{61}BM$ as an acceptor were analyzed. A small optimization study with different donor to acceptor ratios indicated a 1:3 ratio gave the highest light currents. Using this 1:3 ratio, the optimal processing solvent was determined by measuring the EQE for regular, non-cavity enhanced OPD devices. Active layers processed from chlorobenzene (CB) and chloroform (CF) afforded higher EQE values than those processed from *ortho*-dichlorobenzene (*o*-DCB) (**Figure S8**). Even though the EQE patterns of the devices processed from CF and CB are very similar, atomic force microscopy (AFM, **Figure S9**) showed a rougher active layer for CF-processed layers (root-mean-square value (Rq) of 0.68 nm compared to 0.45 nm for the ones spin-coated from CB). Furthermore, optical microscopy images of blends processed from CF showed wave-like thickness variations on a scale of 5 to 10 µm, while the layers processed from CB afforded a more uniform thickness (**Figure S10**). As the resonance wavelength of cavity enhanced devices is determined by the active layer thickness, thickness variations in the active layers have to be kept minimal in order to achieve sharp resonances. Therefore, CB was selected as the optimal processing solvent.

To compare the performance of optimized PTTPQx:$PC_{61}BM$ (1:3) and PDTPQx:$PC_{61}BM$ (1:4) photoactive layers in standard OPD devices, using CB and CF as solvents, we measured current-voltage curves in darkness and under illumination (**Figure 3a** and **b**). Relevant parameters are listed in **Table 2**. In this case, the illumination source was a solar simulator. Even though this is a broadband light source, a fair comparison between photocurrents can still be made, since the absorption spectra of PTTPQx and PDTPQx are similar (**Figure 2**).

While the open-circuit voltages (V_{OC}) differ only slightly, by 30 mV, the photocurrent density (J_{Ph}) for the PTTPQx:$PC_{61}BM$ blend (1.4×10^{-2} A cm^{-2}) is twice as large as the one for the PDTPQx:$PC_{61}BM$ blend (5.6×10^{-3} A cm^{-2}), consistent with a doubled EQE (peaking at 47% in the NIR as compared to 20%; **Figure 3c**). The internal quantum efficiency (IQE) determined from **Figure 3d** shows a significantly better result for the PTTPQx-based blend, with an IQE of 0.79 compared to 0.35 for the PDTPQx-based blend.

From the absolute values of the V_{OC} and J_{Ph}, a theoretical lower limit for the absolute value of the dark current density at reverse voltages can be calculated:[35]

$$J_D > J_{Ph} e^{-V_{OC}\frac{q}{kT}}$$

Since both polymer blends show a similar V_{OC}, these theoretical lower limits are in the same order of magnitude, ~5 x 10^{-9} A cm^{-2}. However, the measured dark current at -1 V is 2 x 10^4 times higher than the lower limit for the PDTPQx:PC_{61}BM active layer, whereas it is only 50 times higher for the PTTPQx:PC_{61}BM blend. PTTPQx therefore clearly outperforms PDTPQx, both in terms of dark current and EQE.

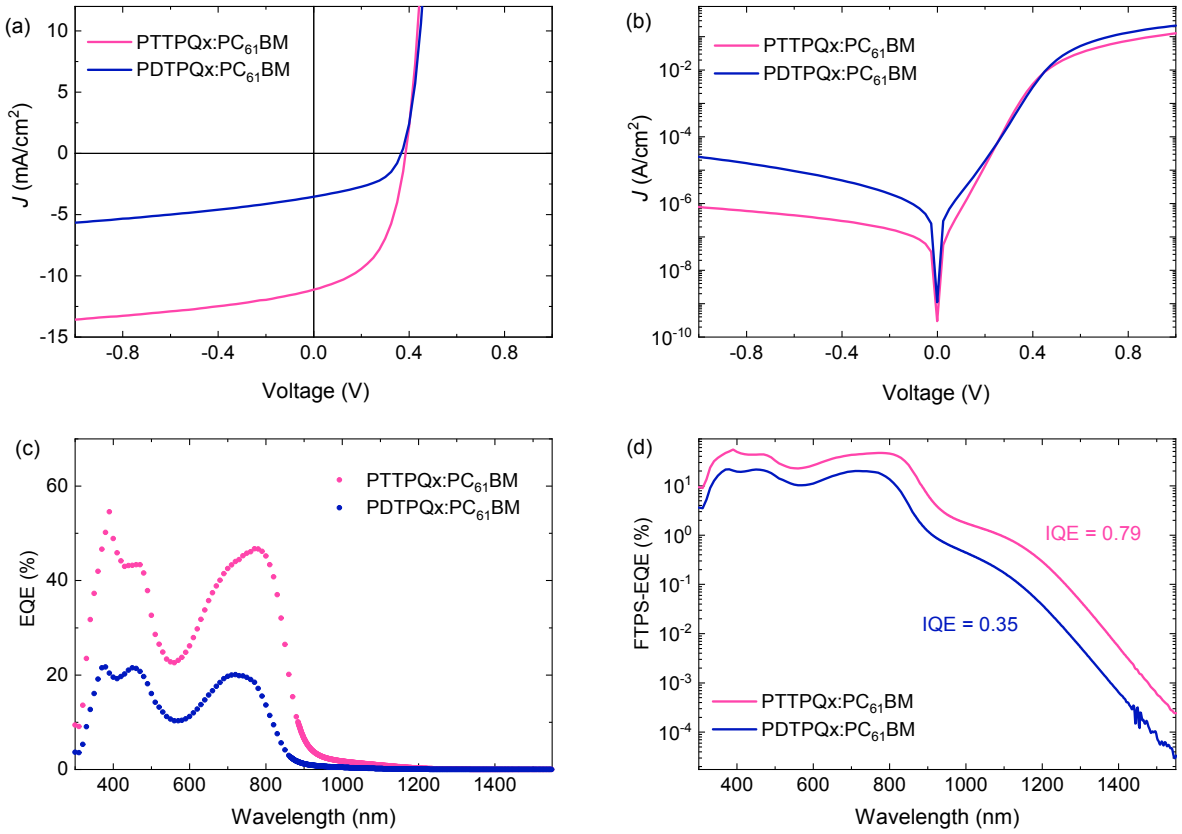

Figure 3: *J-V* curves measured (a) under illumination and (b) in the dark and regular (c) and sensitive (d) external quantum efficiencies for the optimized OPD devices based on PDTPQx (blue) and PTTPQx (pink) in blends with PC_{61}BM (1:4 and 1:3, respectively). Active layer thicknesses were 110 and 125 nm for the PDTPQx- and PTTPQx-based devices, respectively.

Table 2: Overview of the obtained E_{CT}, V_{OC}, J_{Ph}, and J_D values for PTTPQx and PDTPQx blended with PC_{61}BM in regular (ITO) devices and the calculated V_{OC}-limited dark current, $J_{D,V_{OC}}$.

Blend	E_{CT} (eV)	V_{OC} (V)	J_{Ph} (A cm^{-2})	J_D (at -1 V) (A cm^{-2})	$J_{D,V_{OC}}$ (A cm^{-2})	μ (cm^2 V^{-1} s^{-1})
PDTPQx:PC_{61}BM (1:4)	1.06	0.36	5.6 × 10^{-3}	2.7 × 10^{-5}	5.0 × 10^{-9}	2.6 x 10^{-4}
PTTPQx:PC_{61}BM (1:3)	1.01	0.39	1.4 × 10^{-2}	7.8 × 10^{-7}	3.9 × 10^{-9}	2.3 x 10^{-3}

To shed light on this performance difference, hole mobilities of both blends were investigated by measuring current-voltage curves on hole-only devices (**Table 2, Figure S11**). With a similar active layer thickness, the PTTPQx:PC_{61}BM blend showed a hole mobility of 2.3 x 10^{-3} cm^2 V^{-1} s^{-1}, which is almost ten times higher than the value obtained for the PDTPQx:PC_{61}BM blend (2.6 x 10^{-4} cm^2 V^{-1} s^{-1}) and can explain the higher IQE of these devices. This difference originates from the difference in hole mobility for the neat polymer materials. For a pristine PTTPQx film, a hole mobility of 1.8 x 10^{-3} cm^2 V^{-1} s^{-1} was

found, which is around 40 times higher than the value obtained for a pure PDTPQx film (4.3 x 10^{-5} cm^2 V^{-1} s^{-1}) (**Figure S11**).

Furthermore, the higher IQE values of the PTTPQx:$PC_{61}BM$ blend suggest this material to be better suitable for the purpose of cavity-based photodetectors. Previous work concerning these devices showed that intermixing of the donor and acceptor materials is crucial to obtain strong CT absorption.[25,26] For polymeric materials, intercalation of the fullerene acceptor molecules, hereby forming a bimolecular co-crystal, has resulted in strong CT absorption.[25,26] Thus, to examine the structure and signatures of intercalation/intermixing, grazing-incidence wide angle X-ray scattering (GIWAXS) was used to examine the ordering of PDTPQx and PTTPQx in the neat state (**Figure 4a**) and when blended with $PC_{61}BM$ (**Figure 4b**). Both the PDTPQx and PTTPQx polymer are largely isotropic, with little long-range ordering. The increased scattering intensity for PTTPQx indicates a larger degree of long-range ordering in this polymer (**Figure S12**). When blended in a 1:3 ratio with $PC_{61}BM$, the long-range ordering attributed to PTTPQx disappears and only scattering from amorphous $PC_{61}BM$ is observed (**Figure S13**). Conversely, the lamellar stacking peak at Q_{xy} = 0.28 $Å^{-1}$ (**Figure 4b**) from neat PDTPQx is retained after blending with $PC_{61}BM$, suggesting the presence of a neat polymer phase within the blend. The $PC_{61}BM$ signals at Q_{xy} = 0.71 $Å^{-1}$ and 1.39 $Å^{-1}$ also appear more pronounced in the PDTPQx:$PC_{61}BM$ blend, which is consistent with less intermixing of the two components. These results suggest that rather than phase separating into pure components, PTTPQx appears to better intermix with $PC_{61}BM$, leading to a more amorphous blend. The origin for the higher hole mobility of the PTTPQx:$PC_{61}BM$ blend, despite its more amorphous nature (and the comparably lower molar mass of PTTPQx), may thus be in the more delocalized PTTPQx backbone electronic wavefunction due to the addition of the two fused thiophene units. Water contact angle measurements (**Figure S14**) were performed and showed little to no polarity difference between the two donor polymers.

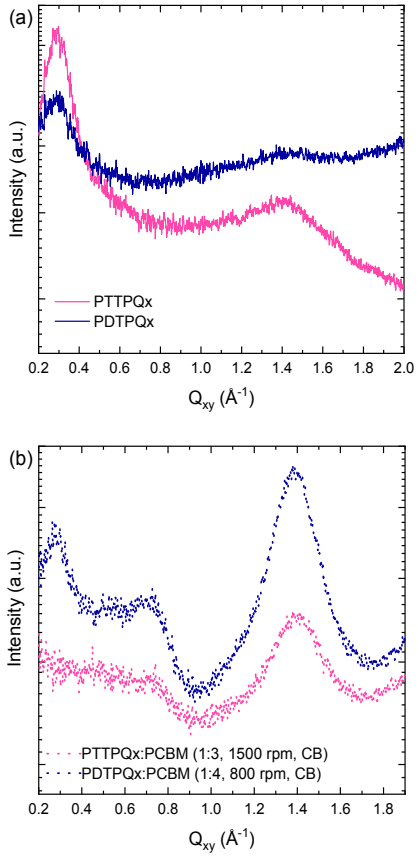

Figure 4: Q_{xy} lineouts from GIWAXS analysis for (a) the PDTPQx and PTTPQx pristine polymers, and (b) the polymers blended with $PC_{61}BM$. The broad peak at 0.29 $Å^{-1}$ is attributed to the lamellar stacking of the polymer, whereas the features at 0.71 $Å^{-1}$ and 1.39 $Å^{-1}$ are assigned to $PC_{61}BM$.

The CT absorption band onset was fitted with a Gaussian function derived from Marcus theory (**Figure 5**, **Table S1**).[36,37] From this, the energy of the CT state, E_{CT}, could be determined. The difference in E_{CT} between the two blends is only 0.05 eV, which agrees well with the small difference in HOMO energy levels (0.03 eV; **Table 2**).

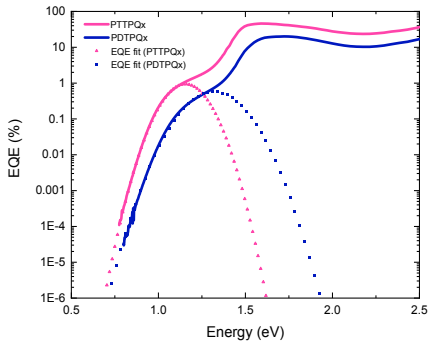

Figure 5: External quantum efficiency versus energy and the fitted curves (dashed lines), illustrating decreasing E_{CT} gaps of 1.06 and 1.01 eV for PDTPQx and PTTPQx, respectively (see SI for fitting details).

The high IQEs and relatively low dark currents for the PTTPQx:$PC_{61}BM$ blend, combined with the enhanced intermixing between the new polymer and $PC_{61}BM$, encouraged us to implement this material combination in a resonant optical cavity photodetector. Optical transfer-matrix simulations were carried out using the refractive index (n) and absorption coefficient (k) of the polymer (**Figure**

S15). These simulations showed a narrowband photoresponse for this active layer with a thickness between 130 and 270 nm (**Figure S16**). Therefore, six different thicknesses between 135 and 285 nm were investigated in the cavity photodetector device stack (glass/Au/Ag/ZnO/active layer/MoO_3/Ag) and all performance parameters are given in **Table S2**. EQEs from 23% at 921 nm to 0.2% at 1448 nm were achieved, with a FWHM between 32 and 40 nm and thermal (Johnson) noise limited detectivities ranging from 1.07 x 10^{12} to 1.82 x 10^{10} Jones at 0 V (**Figure 6**). These results, indicated as pink diamonds in **Figure 7**, outperform the ones achieved for the PDTPQx-based devices (indicated as blue triangles) and are among the best detectivities overall within this wavelength range.

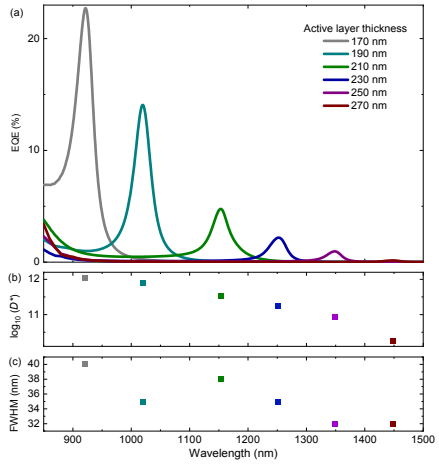

Figure 6: (a) EQE, (b) detectivity, and (c) FWHM for the PTTPQx:PC_{61}BM cavity photodetector devices with increasing active layer thickness.

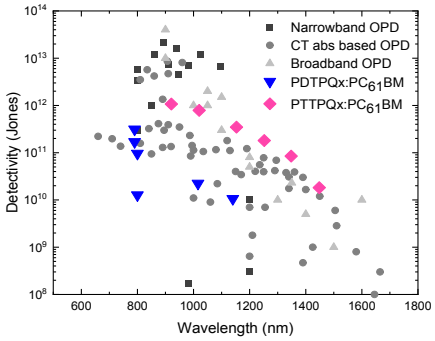

Figure 7: Overview of reported detectivities for narrowband OPDs (■), CT absorption-based OPDs (●), and broadband OPDs (Δ), illustrating that the results for our PTTPQx-based devices (pink diamonds) are among the best in the wavelength range from 1100 to 1450 nm, clearly outperforming the PDTPQx-based devices (blue triangles).[22,26,27]

Conclusions

A novel ladder-type conjugated polymer, PTTPQx, was successfully synthesized and compared to a previously reported PDTPQx polymer with a slightly different (*i.e.* less extended) electron-donating monomer. Even though the characteristics of the pure polymers (molar mass, energy levels, absorption spectrum) are very much alike, there is a clear performance difference in bulk heterojunction photodiode devices. PTTPQx showed a higher external quantum efficiency and lower dark current when combined with PC_{61}BM as the active material in an inverted photodiode stack. These performance differences can be attributed to the higher hole mobility (by one order of magnitude) and the slightly enhanced intermixing for the PTTPQx:PC_{61}BM devices. When applied in an optical cavity photodetector, peak external quantum efficiencies from 23% at 921 nm to 0.2% at 1448 nm, with a full-width-at-half-maximum between 32 and 40 nm, were obtained. Furthermore, specific

detectivities ranging from 1.07 x 10^{12} to 1.82 x 10^{10} Jones were realized, which are among the best values achieved to date for this near-infrared wavelength range.

Acknowledgements

The authors thank Huguette Penxten for the CV analysis and Prof. Alberto Salleo for his support in the GIWAXS analysis. They also thank the Research Foundation – Flanders (FWO Vlaanderen) for continuing financial support (PhD scholarships 1S98320N, 1S50822N, projects G0D0118N, G0B2718N, 1S50820N, 11D2618N, and the Scientific Research Network 'Supramolecular chemistry and materials'), as well as the European Research Council (ERC, grant agreement 864625). Q.L. acknowledges financial support from the European Union's Horizon 2020 research and innovation program under the Marie-Curie grant agreement no. 882794. T.J.Q. acknowledges support from the National Science Foundation Graduate Research Fellowship Program under grant DGE-1656518. This material is based upon work supported by the U.S. Department of Energy, Office of Science, Office of Workforce Development for Teachers and Scientists, Office of Science Graduate Student Research (SCGSR) program. The SCGSR program is administered by the Oak Ridge Institute for Science and Education for the DOE under contract number DE-SC0014664. Use of the Stanford Synchrotron Radiation Light source, SLAC National Accelerator Laboratory, is supported by the U.S. Department of Energy, Office of Science, Office of Basic Energy Sciences under Contract No. DE-AC02-76SF00515. Part of this work was performed at the Stanford Nano Shared Facilities (SNSF), supported by the National Science Foundation under award ECCS-2026822.

Author contributions

Kaat Valkeneers: investigation (materials synthesis and characterization), funding acquisition, visualization, writing – original draft, writing – review & editing

Jorne Raymakers: investigation (materials synthesis and characterization), funding acquisition, writing – review & editing

Quan Liu: investigation (cavity photodetectors), funding acquisition, visualization, writing – review & editing

Jochen Vanderspikken: investigation (GIWAXS), writing – review & editing

Yuming Wang: investigation (mobility), writing – review & editing

Jurgen Kesters: investigation (photodetectors), writing – review & editing

Tyler James Quill: investigation (GIWAXS), writing – review & editing

Zhen Liu: investigation (thermal analysis), writing – review & editing

Niko Van den Brande: supervision (thermal analysis), writing – review & editing

Laurence Lutsen: supervision, funding acquisition, writing – review & editing

Koen Vandewal: conceptualization, supervision (photodetector part), funding acquisition, writing – review & editing

Wouter Maes: conceptualization, project administration, supervision (polymer synthesis and characterization part), funding acquisition, writing – review & editing

Conflict of Interest

The authors declare no conflict of interest.

References

1 M. Yang, Z. Yang, T. Yuan, W. Feng and P. Wang, Front. Neurol., 2019, 10, 58.

2 J. Huang, J. Lee, J. Vollbrecht, V. V Brus, A. L. Dixon, D. X. Cao, Z. Zhu, Z. Du, H. Wang, K. Cho, G. C. Bazan and T. Q. Nguyen, Adv. Mater., 2020, 32, 1906027.

3 H. Chen, A. Chen, L. Xu, H. Xie, H. Qiao, Q. Lin and K. Cai, Agric. Water Manag., 2020, 240, 106303.

4 K. Sendin, P. J. Williams and M. Manley, Crit. Rev. Food Sci. Nutr., 2018, 58, 575–590.

5 G. Hong, A. L. Antaris and H. Dai, Nat. Biomed. Eng., 2017, 1, 1–22.

6 T. Yokota, K. Fukuda and T. Someya, Adv. Mater., 2021, 33, 2004416.

7 A. Sudhaik, A. A. Parwaz Khan, P. Raizada, V. H. Nguyen, Q. Van Le, A. M. Asiri and P. Singh, Chemosphere, 2022, 291, 132781.

8 J. Xia, F. Zhu, J. Bounds, E. Aluauee, A. Kolomenskii, Q. Dong, J. He, C. Meadows, S. Zhang and H. Schuessler, J. Appl. Phys., 2022, 131, 220901.

9 Y. Song, G. Yu, B. Xie, K. Zhang and F. Huang, Appl. Phys. Lett., 2020, 117, 093302.

10 S. J. Xu, S. J. Chua, T. Mei, X. C. Wang, X. H. Zhang, G. Karunasiri, W. J. Fan, C. H. Wang, J. Jiang, S. Wang and X. G. Xie, Appl. Phys. Lett., 1998, 73, 3153–3155.

11 Y. Berencén, S. Prucnal, F. Liu, I. Skorupa, R. Hübner, L. Rebohle, S. Zhou, H. Schneider, M. Helm and W. Skorupa, Sci. Rep., 2017, 7, 1–9.

12 H. Bronstein, C. B. Nielsen, B. C. Schroeder and I. McCulloch, Nat. Rev. Chem., 2020, 4, 66–77.

13 F. Verstraeten, S. Gielen, P. Verstappen, J. Raymakers, H. Penxten, L. Lutsen, K. Vandewal and W. Maes, J. Mater. Chem. C, 2020, 8, 10098–10103.

14 F. Verstraeten, S. Gielen, P. Verstappen, J. Kesters, E. Georgitzikis, J. Raymakers, D. Cheyns, P. Malinowski, M. Daenen, L. Lutsen, K. Vandewal and W. Maes, J. Mater. Chem. C, 2018, 6, 11645–11650.

15 J. Vanderspikken, W. Maes and K. Vandewal, Adv. Funct. Mater., 2021, 31, 2104060.

16 Y. Wang, J. Kublitski, S. Xing, F. Dollinger, D. Spoltore, J. Benduhn and K. Leo, Mater. Horizons, 2022, 9, 220–251.

17 X. Huang, N. Lan, W. Chen, Y. Yan, W. Zeng and S. Liu, J. Mater. Sci., 2021, 56, 8334–8357.

18 P. Jacoutot, A. D. Scaccabarozzi, D. Nodari, J. Panidi, Z. Qiao, A. Schiza, A. D. Nega, A. Dimitrakopoulou-Strauss, V. G. Gregoriou, M. Heeney, C. L. Chochos, A. A. Bakulin and N. Gasparini, Sci. Adv., DOI:10.1126/SCIADV.ADH2694.

19 A. E. London, L. Huang, B. A. Zhang, M. B. Oviedo, J. Tropp, W. Yao, Z. Wu, B. M. Wong, T. N. Ng and J. D. Azoulay, Polym. Chem., 2017, 8, 2922–2930.

20 Q. Lin, A. Armin, P. L. Burn and P. Meredith, Nat. Photonics, 2015, 9, 687–694.

21 A. Yazmaciyan, P. Meredith and A. Armin, Adv. Opt. Mater., 2019, 7, 1801543.

22 Q. Liu, S. Zeiske, X. Jiang, D. Desta, S. Mertens, S. Gielen, R. Shanivarasanthe, H. G. Boyen, A. Armin and K. Vandewal, Nat. Commun. 2022, 13, 1–11.

23 B. Siegmund, A. Mischok, J. Benduhn, O. Zeika, S. Ullbrich, F. Nehm, M. Böhm, D. Spoltore, H. Fröb, C. Körner, K. Leo and K. Vandewal, Nat. Commun., 2017, 8, 1–6.

24 J. Yang, J. Huang, R. Li, H. Li, B. Sun, Q. Lin, M. Wang, Z. Ma, K. Vandewal and Z. Tang, Chem. Mater., 2021, 33, 5147–5155.

25 Z. Tang, Z. Ma, A. Sánchez-Díaz, S. Ullbrich, Y. Liu, B. Siegmund, A. Mischok, K. Leo, M. Campoy-Quiles, W. Li and K. Vandewal, Adv. Mater., 2017, 29, 1702184.

26 J. Vanderspikken, Q. Liu, Z. Liu, T. Vandermeeren, T. Cardeynaels, S. Gielen, B. Van Mele, N. Van den Brande, B. Champagne, K. Vandewal and W. Maes, Adv. Funct. Mater., 2022, 32, 2108146.

27 T. Vandermeeren, Q. Liu, S. Gielen, D. Theunissen, S. Frederix, M. Van Landeghem, Z. Liu, N. Van den Brande, J. D'Haen, J. Vanderspikken, L. Lutsen, K. Vandewal and W. Maes, Dye. Pigment., 2022, 200, 110130.

28 W. Huang, W. Xie, H. Huang, H. Zhang and H. Liu, J. Phys. Chem. Lett., 2020, 11, 4548–4553.

29 Y. Wang, H. Guo, S. Ling, I. Arrechea-Marcos, Y. Wang, J. T. López Navarrete, R. P. Ortiz and X. Guo, Angew. Chemie - Int. Ed., 2017, 56, 9924–9929.

30 C. K. Wang, B. H. Jiang, J. H. Lu, M. T. Cheng, R. J. Jeng, Y. W. Lu, C. P. Chen and K. T. Wong, ChemSusChem, 2020, 13, 903–913.

31 B. Zhao, C. Yan, Z. Wang, H. Huang, Y. Hu, P. Cheng, M. Yi, C. Huang, X. Zhan and W. Huang, J. Mater. Chem. C, 2017, 5, 8988–8998.

32 DE102013110693A1, 2015.

33 J. T. Henssler and A. J. Matzger, Org. Lett., 2009, 11, 3144–3147.

34 L. Marin, L. Lutsen, D. Vanderzande and W. Maes, Org. Biomol. Chem., 2013, 11, 5866–5876.

35 S. Gielen, C. Kaiser, F. Verstraeten, J. Kublitski, J. Benduhn, D. Spoltore, P. Verstappen, W. Maes, P. Meredith, A. Armin, K. Vandewal, S. Gielen, F. Verstraeten, P. Verstappen, W. Maes, K. Vandewal, C. Kaiser, P. Meredith, A. Armin, J. Kublitski, J. Benduhn and D. Spoltore, Adv. Mater., 2020, 32, 2003818.

36 K. Vandewal, K. Tvingstedt, A. Gadisa, O. Inganäs and J. V. Manca, Phys. Rev. B - Condens. Matter Mater. Phys., 2010, 81, 125204.

37 R. A. Marcus, J. Phys. Chem., 1989, 93, 3078–3086.